

Simulation method for highly entangled polymer nanocomposites: scaling exponents of Slip-Spring age among free and grafted chains, grafting density and nanoparticle/polymer interaction dependence on particle dispersion.

Semen VASIN^{1,2}, Gaetan MAUREL¹, Taiji MIKAMI¹, Corentin HERMANGE¹, Iurii CHUBAK¹, Robert J. Tannenbaum¹, Sarah C. SEEGER¹, Catherine GAUTHIER², and Marc COUTY^{1*}

1. Manufacture Française des Pneumatiques MICHELIN 23, place des Carmes-Déchaux F-63000 Clermont-Ferrand, France
2. INSA Lyon, CNRS, MATEIS, UMR5510, F-69621 Villeurbanne, France

Supplementary information on the properties of pure polymer systems

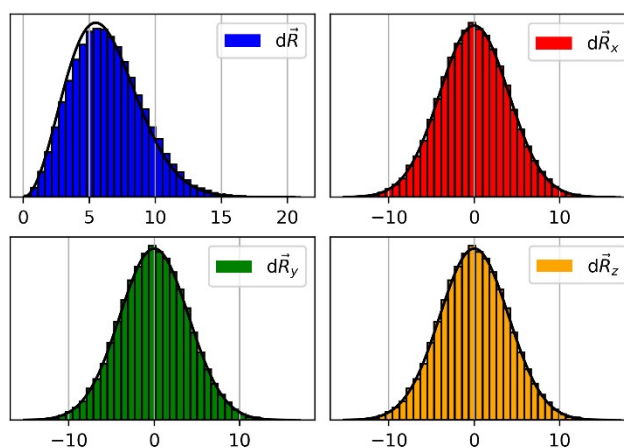


Figure S1. Distribution of length of end-to-end vectors (top left) and x,y and z components (top right, bottom left and bottom right correspondingly).

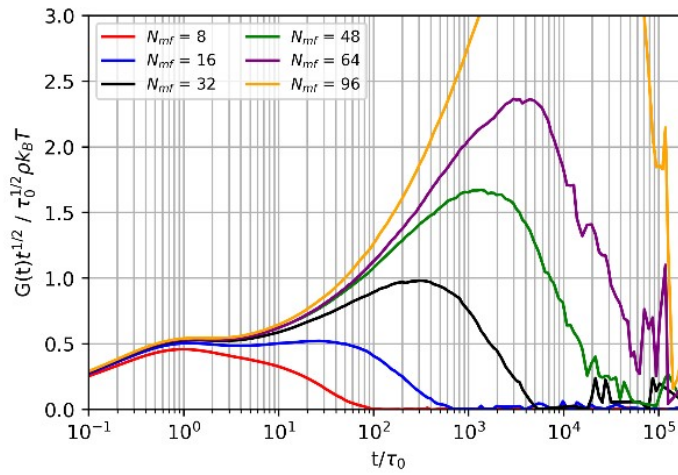


Figure S2. $G(t)t^{1/2}$ versus t for pure polymer melts of different chain lengths.

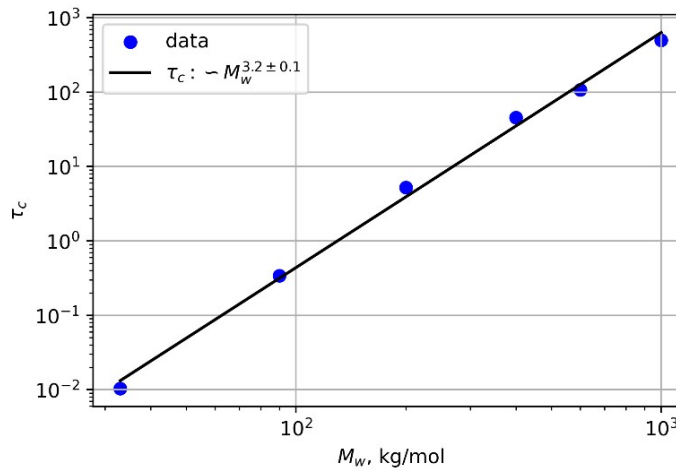


Figure S3. Fitting dependence of G' and G'' crossing points on polymer molecular weight with a power law. Data extracted from work of Auhl *et al.*

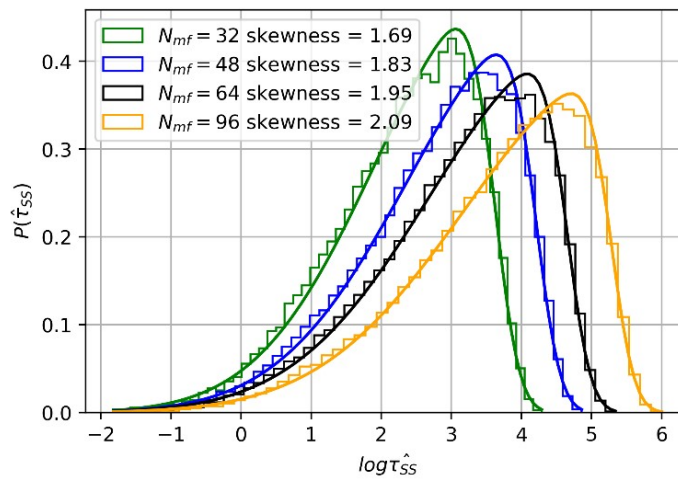


Figure S4. SS age probability density for pure polymer of different length and fitting with skewnormal distribution. Skewness coefficients are indicated in the legend.

Diffusion coefficient computation

To investigate the effect of the melt chain length and the NP size on the NP diffusion we additionally simulate the diffusion of a single nanoparticle of different size ($R_{NP} = 2, 3, \text{ and } 4b$) in an entangled polymer matrix with chains of different length lengths from 24 to 96 beads for more than 10 independent runs. We compute the nanoparticle diffusion coefficient using the linear region of long-

$$\langle (r(t) - r_0)^2 \rangle = 6Dt \quad (1)$$

time MSD as follows:

For the sake of consistency for simulations of particles of different size, we have not applied the corrections for the finite box size. The NPs were simulated in a box of at least two times its diameter.

In Figure S5A, we show the MSD for bare and grafted fillers with $\epsilon = 0$ and $\epsilon = -0.6k_B T$ and extract diffusion coefficients using Eq. (1). The diffusion coefficient somewhat reduces with the filler friction coefficients ξ (less than by 40-50% for considered bare and grafted fillers when ξ is increased by a factor of 10), we conclude thus that the chosen values are sufficiently large to ensure well overdamped NP dynamics. The diffusion of grafted nanoparticles is more suppressed (Figure S5B), which can be explained by the fact that the introduction of grafted chains creates additional obstacles to free diffusion due to entanglements between free and grafted chains, thereby modifying the effective nanoparticle radius and local system viscosity with respect to the bulk melt². The MSD curves in Figure S5C-D show that longer chains with higher viscosity (see inserts from Figure 2A of the main text) considerably decelerate NP diffusion (Figure S5C). A similar effect is observed when comparing different NP radii (Figure S5D) with the diffusion being hindered for larger R_{NP} .

We now compare our case with the simulations of Kalathi et al³. First, we note that the tube diameter $d_T \approx b\sqrt{N_e} = 2b$ in our case, so we are constantly in a regime of strong coupling between the dynamics of NPs and the entanglement network. In Fig. S6, we report D as function of N in different

representations, consistent with the Ref. 3. We find that D reduces with the melt chain length N_{mf} and with the nanoparticle radius R_{NP} (Fig. S5C). When plotting $D8R_{NP}^3$ versus $N_{mf}/4R_{NP}^2$, (Fig. S6B) our data overlaps fairly but no plateau is found at large N_{mf} , reproducing the well-entangled case of the Ref. 3 ($\sigma_{NP} > 8\sigma$). To prove that effect of entanglement is indeed at the core of the observed slow-down of diffusion, we computed D for nanoparticles with $R_{NP} = 3$ embedded in a non-entangled matrix (without slip-springs) with $N_{mf} = 24, 48,$ and 96 . As seen from our results (green stars on Fig. S6B), D in such systems effectively does not depend on N_{mf} reproducing the effect seen in Ref. 3 for the Stokes-Einstein regime of NPs of size much smaller than chain but much larger than d_T , and the entangled system shows a much more suppressed diffusion. The macroscopic Stokes-Einstein relation is expected to recover in the limit of NPs size much larger than chain size and d_T . Similarly to the Ref. 3, we find that $D\eta R_{NP}$ increases faster with varying N_{mf} , indicating a pronounced effect of entanglement (Fig. S6A). To access the macroscopic Stokes-Einstein regime, we would need to simulate systems with much shorter chains in boxes with a much bigger size to reduce the effect of periodic boundary conditions. In summary, we have shown that our simulation approach reproduces the results of Ref. 3 for the NP diffusion in the case of well-entangled matrices when the NP size is comparable or smaller to that of d_T .

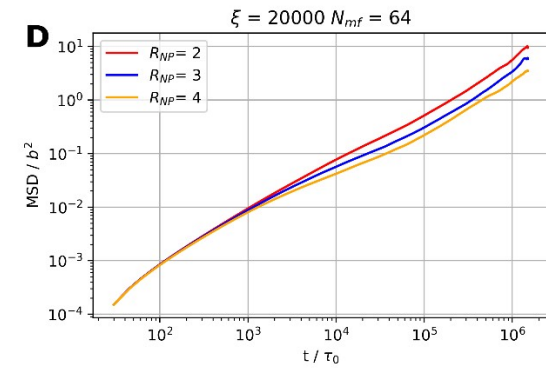
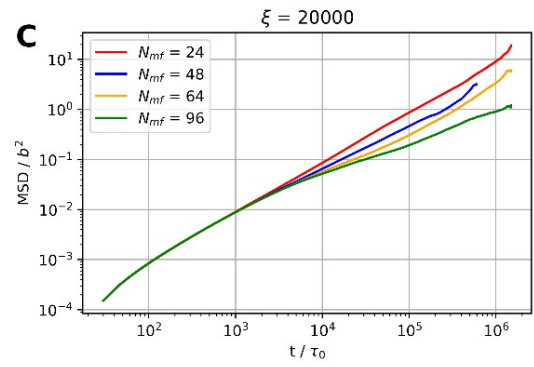
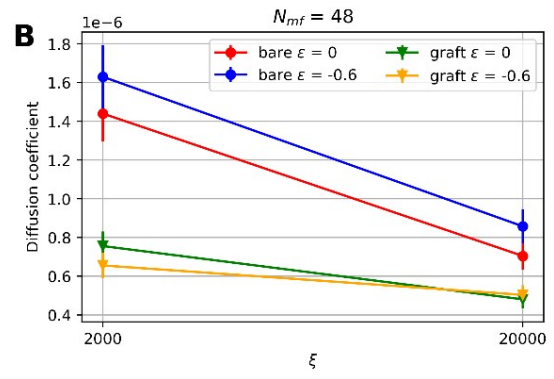
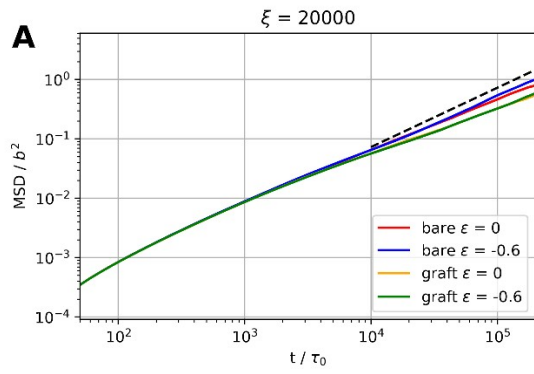


Figure S5. (A) Mean square displacement for bare and grafted fillers (grafting density $\sigma = 0.2b^{-2}$) with $\epsilon = 0$ and $-0.6k_B T$, respectively, the friction coefficient of filler is $\xi = 20000\tau_0^{-1}$, and $R_{NP} = 3b$. (B) Diffusion coefficients for bare and grafted fillers with $\epsilon = 0$ and $-0.6k_B T$ computed for $\xi = 2000\tau_0^{-1}$ and $20000\tau_0^{-1}$, and $R_{NP} = 3b$. The grafting density is $\sigma = 0.2b^{-2}$, the free and grafted chain lengths are 48. (C) Mean square displacement for different chain lengths of the polymer medium for bare fillers with $R_{NP} = 3b$ and (D) Mean square displacement for different NP radius, $N_{mf} = 64$, $\xi = 20000\tau_0^{-1}$, $\sigma = 0$.

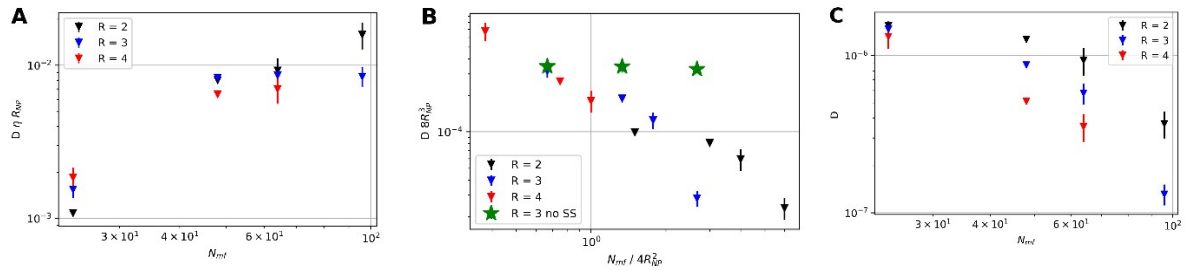


Fig S6. (A) Diffusion coefficient multiplied by the NP radius and viscosity of the medium as a function of polymer chain length N_{mf} , (B) Diffusion coefficient multiplied by the cube of NP diameter of NP as a function of polymer chain length N_{mf} normalized by the square NP diameter and (C) Diffusion coefficients of NP as a function of polymer chain length N_{mf} .

Supplementary information on the properties in nanocomposite systems

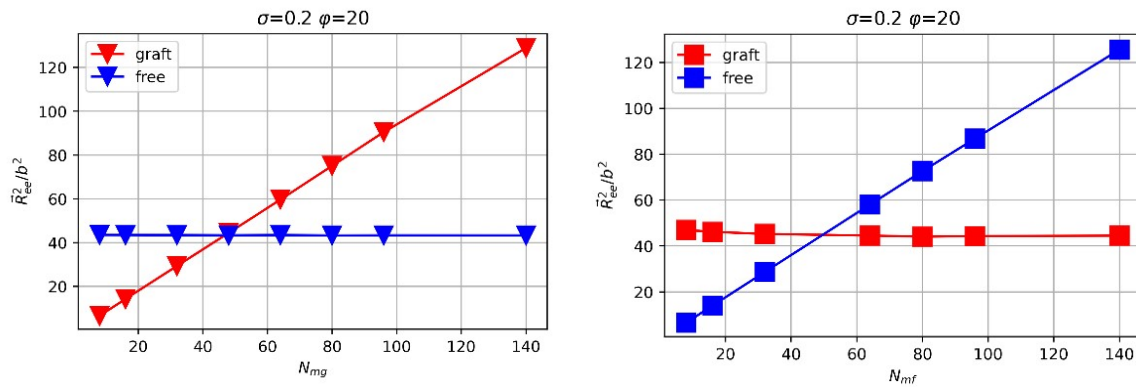


Figure S7. Mean square end-to-end vector \bar{R}_{ee}^2 as a function of grafted chain length N_{mg} with $N_{mf}=48$ (left) and as a function of free chain length N_{mf} with $N_{mg}=48$ (right). Grafting density $\sigma = 0.2 b^{-2}$, volume fraction = 20% and $\epsilon = -0.6 k_B T$.

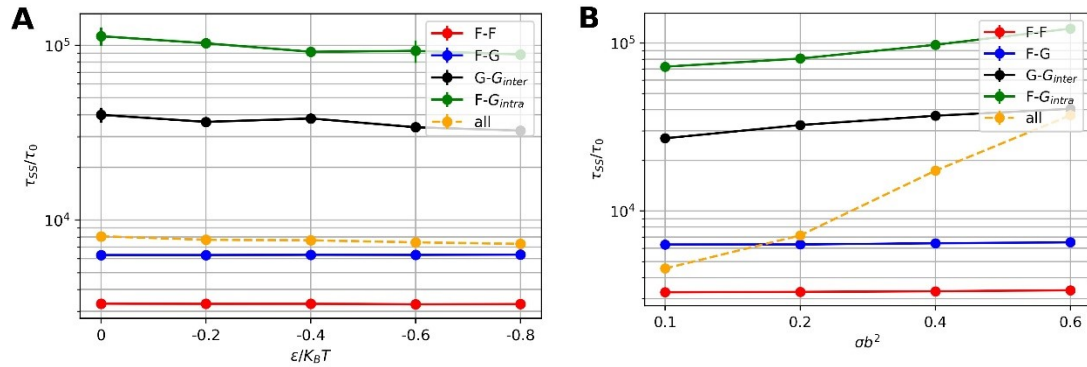


Figure S8. Dependence of the average slip-spring age τ_{SS} (average over 3 independent simulation trials) on (A) different polymer-filler affinity ϵ with grafting density $\sigma = 0.2 b^{-2}$ and (B) grafting density σ with $\epsilon = -0.6 k_B T$. Free and grafted chain lengths are $N_{mf}=48$ $N_{mg}=48$ correspondingly.

Computation of the mean force on fillers

To demonstrate the presence of depletion forces in our modeled systems, we calculate the effective force acting on fillers as a function of distance, using the following protocol.

Initially, a rectangular simulation box is constructed containing two nanoparticles at a specified distance apart. The size of the simulation box is determined based on the volume fraction of fillers, with a volume fraction less than 12% deemed sufficiently large to disregard interactions from fillers in neighboring boxes via boundary conditions.

The study tests ten distinct distances between the surfaces of nanoparticles, specifically: 0.0, 0.2, 0.4, 0.6, 0.8, 1.0, 1.2, 1.4, 1.6, 1.8, 2.0, 2.5, 3.0, 3.5, and 4.0 b . During the direct interactions between fillers (described by Eq. 21 in the main paper) are discarded. Each distance is examined through three parallel simulations, each with different initial configurations of polymers. During these simulations, the fillers are permitted rotational motion but are restricted from translational movement. There are no Slip-Springs added on the chains during Mean Force simulations (effect of the entanglements will be described in the next article).

All simulations commence with 1 million timesteps of relaxation, followed by an additional 100 million timesteps when the average forces acting on the fillers are measured and recorded. By the conclusion of the simulations, effective forces are averaged for each filler. Given the symmetry of the forces, the averages are calculated over both fillers within a single trial. These results are then averaged across three separate trials to determine the final values.

In Figure S8, we show the force acting on the right filler (FOF) for systems with different composition. The measured FOF is that on the right particle, thus negative sign indicates attraction between two fillers. For simplicity, bare fillers were considered. All curves exhibit zones of attraction, followed by repulsion that diminishes at long distances. In Figure S9A, the blue and red curves refer to nanoparticle radii of 2 and 3 b , respectively. Both systems show strong attraction at distances below 1.2 b ; however, the drop in the red curve for bigger fillers is more pronounced, confirming the trend of the Asakura-Oosawa model⁴. Figure S9B shows the effect of free chain length with noticeable differences in the position and intensity of the repulsion peak, making interaction with shorter chains more repulsive at closer distances, again consistent with the Asakura-Oosawa theory. These observations indicate that the described model exhibits expected depletion forces.

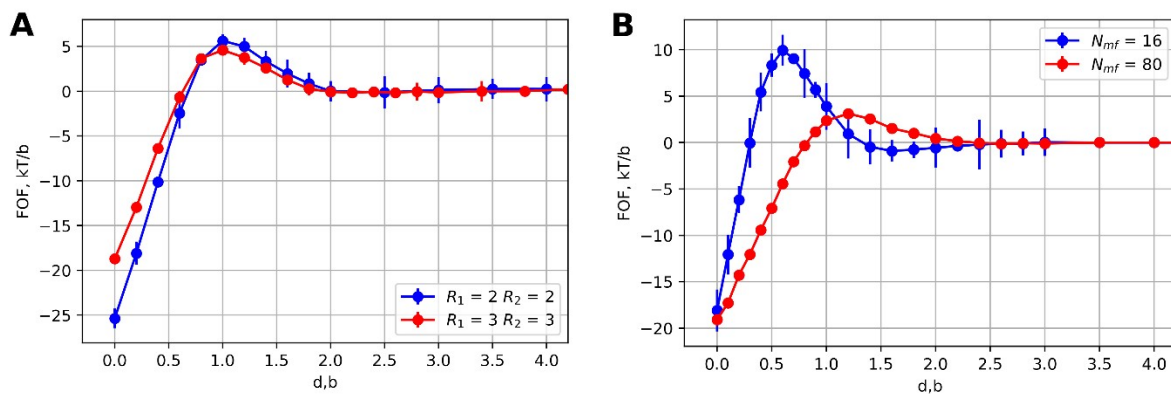


Figure S9. Effective polymer-mediated force acting on fillers along x direction in systems with **(A)** different radius of fillers R and $N_{mf} = 16, \varphi = 12, \sigma = 0, \epsilon = -0.6k_bT$. and **(B)** different free chain length N_{mf} with $R = 2b, \varphi = 12, \sigma = 0, \epsilon = -0.6k_bT$.

Equilibrium structures of non-grafted nanoparticle systems

We show that our simulations can reproduce the relevant states of the phase diagram of bare non-grafted fillers embedded in the polymer melt, as previously reported by K. Schweizer and coworkers by means of PRISM computations^{5,6} as well as MD simulations⁷. More specifically, at melt conditions

close to the protein limit that is relevant for our work, the following equilibrium states of non-grafted fillers have been reported ⁵.

- 1) Phase separation between the fillers and polymer matrix even at very low filler volume fractions in systems with purely repulsive interactions between the filler surface and polymers ($\epsilon = 0$).
- 2) Steric stabilization and good dispersion of fillers in the intermediate range of attraction ϵ due to the formation of adsorbed polymer layers at the filler surface (ϵ of few $k_B T$).
- 3) Tight polymer-bridged network of fillers due to very high attraction ϵ .

We now reproduce such states in our simulations in the case of non-grafted fillers with variable surface affinity ϵ . First, we focus on the case of $N_F = 27$ bare fillers with $\epsilon = 0$ at variable volume fractions. Different volume fractions between 10 and 40% were simulated with chain of length $N_{mf} = 48$ (with 3 independent trials) for up to 200 million simulation steps, and the maximal cluster size as a function of time was traced to probe the binodal (Fig S10). Initially, all the fillers were placed at regular lattice positions. For volume fractions $\phi \geq 20\%$, we systematically find phase separation between the fillers and polymers, as indicated by the formation of a single aggregate in the system over time (snapshots of indicated systems are presented in Fig S11). The cutoff distance in percolation analysis was set at $0.25b$ to capture surface-to-surface contacts. Simulations of systems with $\phi \leq 15\%$ are computationally much more demanding (more than 170k particles in the box), and we were not able to reach fully equilibrium states. Yet, for the volume fraction of 15%, the trend in aggregation is evident (in one of the trials, almost all the particles aggregated in a single cluster during around 150M time steps), indicating the instability of well-mixed filler states. These results are in full agreement with the results published by Zhou et Schweizer⁵. Furthermore, the phase diagram reported by Zhou et Schweizer, indicates phase separation even at marginally small volume fractions in melts at $\epsilon = 0$. We attempted to probe such state by reducing the filler number of filler in the box to $N_F = 20$ at $\phi = 10\%$, yet the system sizes exceed 220k particles and are very slow to simulate with our simulation

code. However, at 10% volume fraction we similarly found an increasing aggregation trend with the maximal cluster size spanning 100% of particles after 80M simulation steps in one of the simulation trials, suggesting instability of the filler phase.

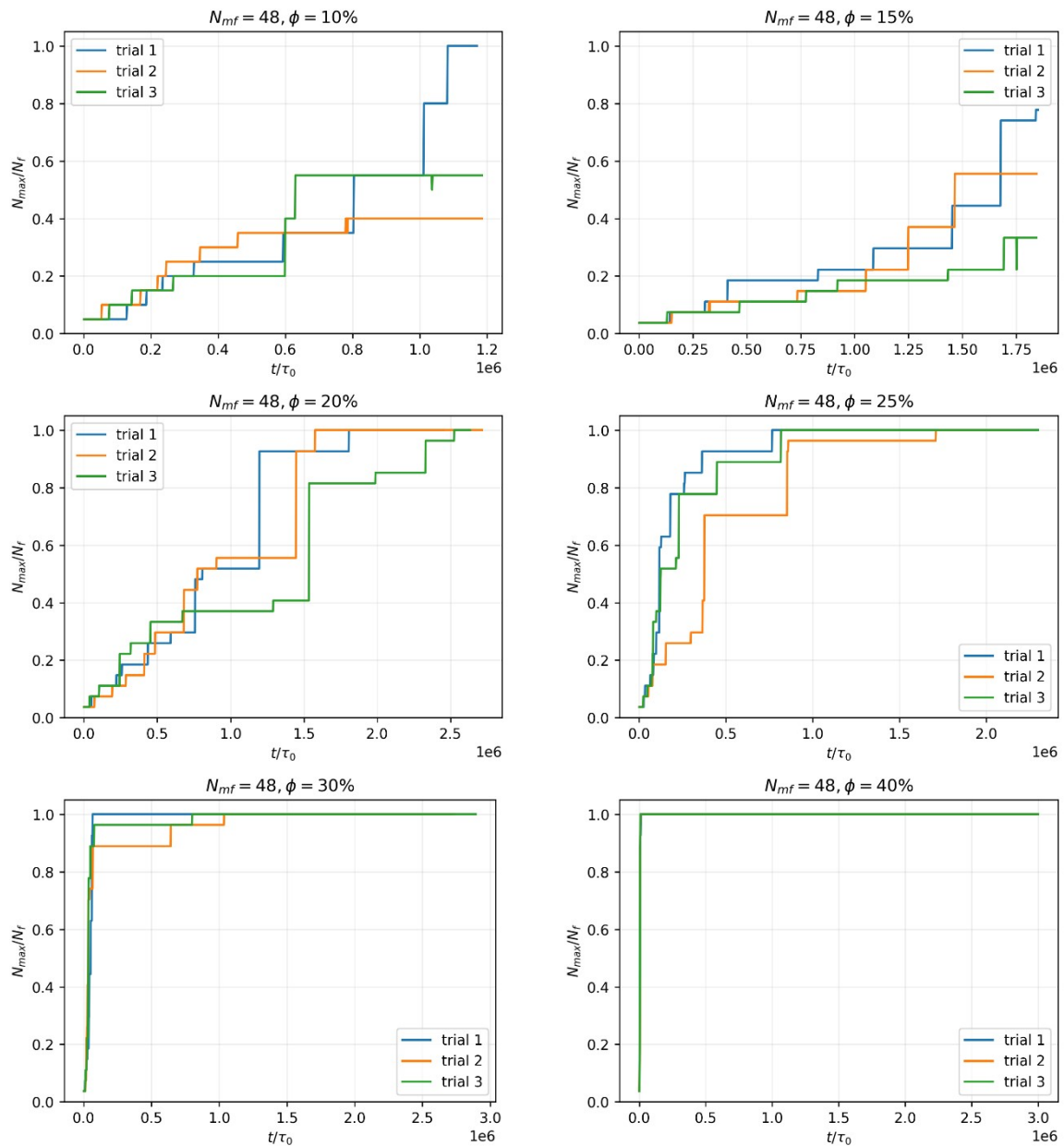


Fig S10. Maximal cluster size as a function of time in systems at variable volume fraction for $\epsilon = 0$, $\sigma = 0$, and $N_{mf} = 48$.

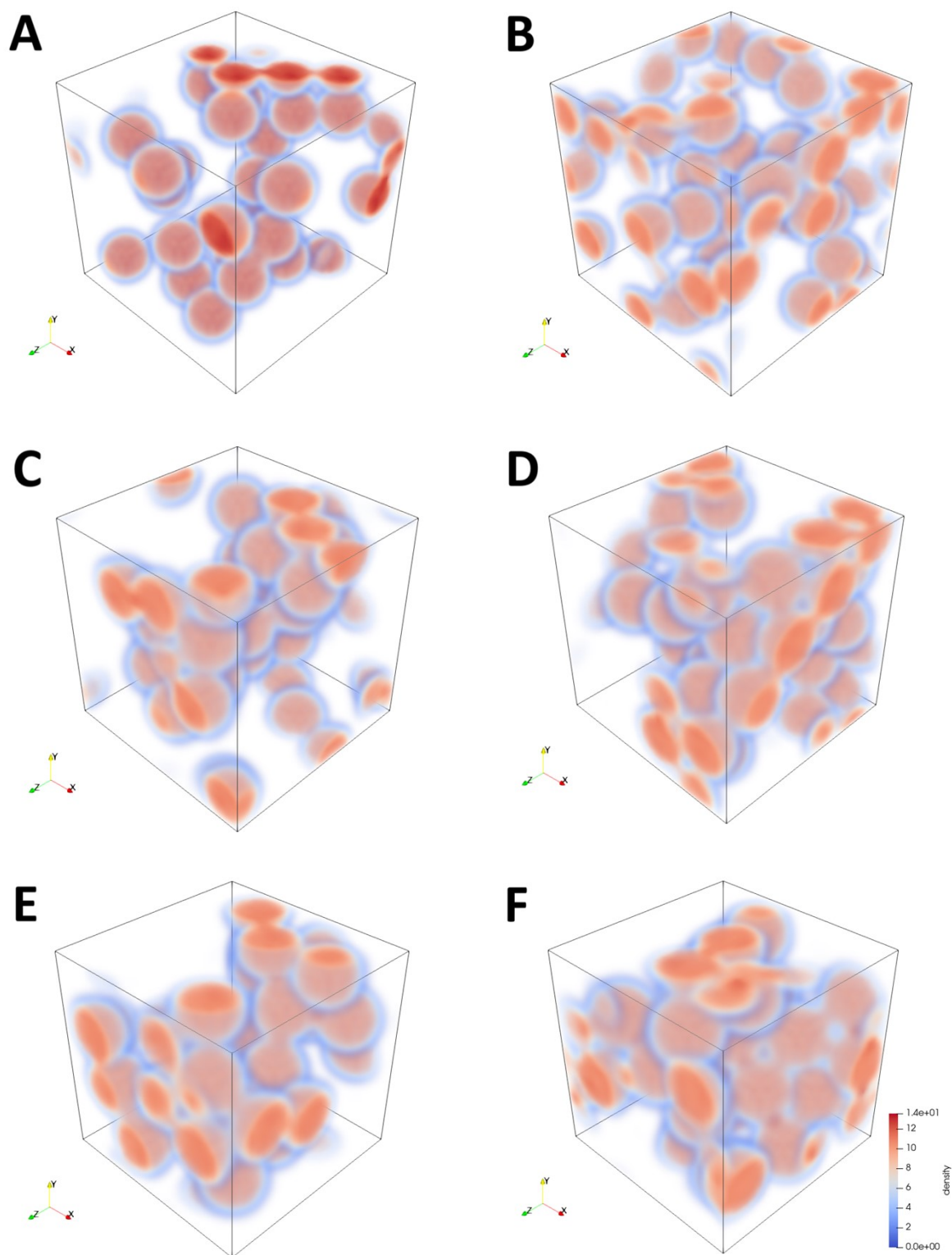


Fig S11. Snapshots of NP configurations with (A) $\phi = 15$ (B) $\phi = 20$ (C) $\phi = 25$ (D) $\phi = 30$ (E) $\phi = 34$ (F) $\phi = 40$. $N_{mf} = 48$, $\epsilon = 0$ and $\sigma = 0$.

We now show that our simulation reproduces the sterically stabilized nanocomposite states reported for higher bare filler attractions⁵. Similarly, we conducted a series of simulations with 27 bare fillers and varying polymer-filler interaction strengths ($\epsilon = 0, -0.4$, and $-0.8 k_B T$), representing increasing attraction between the polymer and filler surface. We present three snapshots of polymer density in the systems (Fig S12 (A-C)) to illustrate that, consistent with results of Zhou et Schweizer, the absence of implicit polymer-filler interaction first results in phase separation (Fig S12 (A)), gradually inducing a stabilized state upon increase attraction (Fig S12 (B) and (C)) due to the formation of an adsorbed polymer layer at the surface. The maximum cluster size for (A) is 27, for (B) 20 and for (C) is 0 NP with respect to the chosen cutoff distance $r_{cut} = 0.25b$. Additionally, we display the radial filler-filler distribution function (Fig S12 (D)), which shows that $\epsilon = 0$ produces a distinct peak at distances close to the NP surface, which diminish with increased filler-polymer attraction. From $\epsilon = -0.6 k_B T$, another peak emerges at a distance close to $2b$, indicating the creation of the network mediated by the polymer absorption layer.

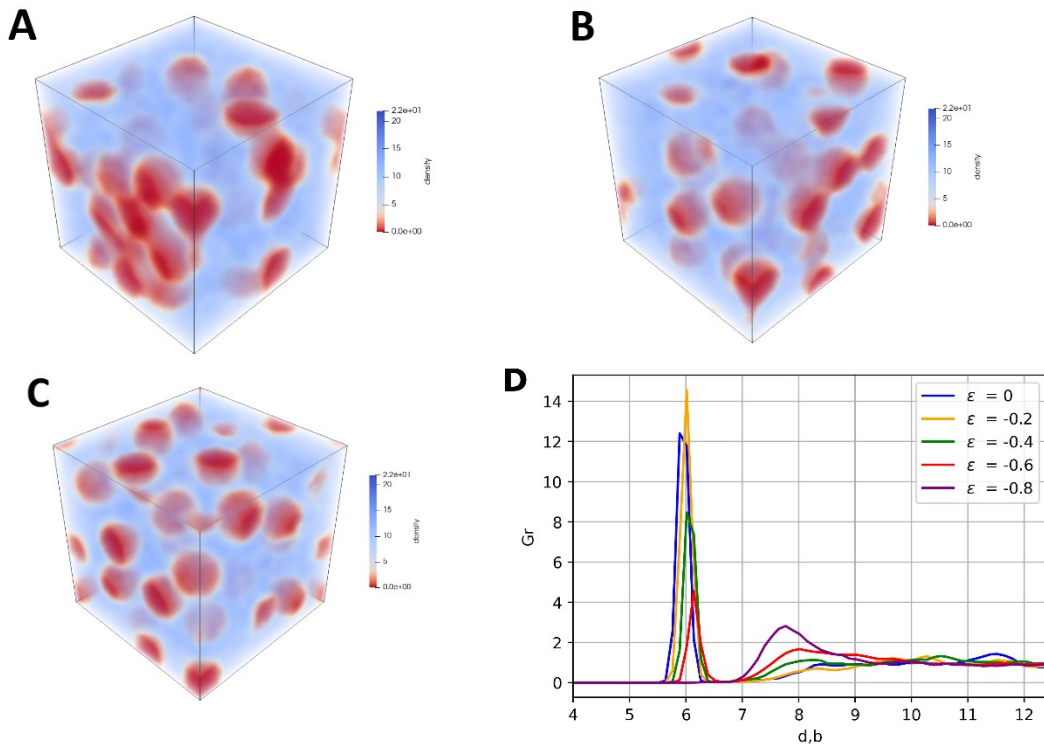


Fig S12. Snapshots of polymer density in systems with (A) $\epsilon=0$ (B) $\epsilon = -0.4 k_B T$ and (C) $\epsilon = -0.8 k_B T$ and (D) Radial distribution function for pairs NP-NP for systems with different ϵ . Other parameters are $\phi = 22$, $\sigma = 0$ and $N_{mf} = 48$.

Finally, we address the nanocomposite morphologies in the case of grafted fillers. In discussing the potential morphologies of polymer-based nanocomposites, it is important to note that defining the morphologies of clusters with 27 nanoparticles (NP) at high volume fractions may not always be convincing. However, there are a few cases where the structures of agglomerates can be clearly distinguished. In the work of Tang and Arya⁸, it was suggested that low grafting densities and relatively short, grafted chain lengths favor the formation of 1D structures, like linear trimers. To confirm, we provide additional snapshots of polymer/filler density for systems with $\epsilon = 0$ and $\sigma = 0.2 \text{ b}^{-2}$ discussed in the main text and can observe that NPs forms linear clusters (as also indicated by nearest neighbor distributions in Figure 6 of the main text).

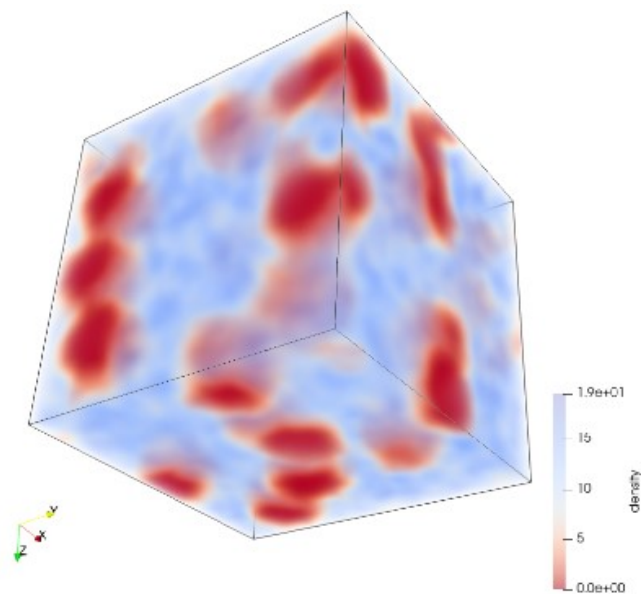


Fig S13. Snapshots of polymer density in system $\epsilon=0$, $\phi = 22$, $\sigma= 0.2 \text{ b}^{-2}$, $N_{mf} = 48$ and $N_{mg}=48$

¹ Auhl D, Ramirez J, Likhtman AE, Chambon P, Fernyhough C. Linear and nonlinear shear flow behavior of

monodisperse polyisoprene melts with a large range of molecular weights. *J Rheol.* 2008;52(3):801-835. doi: 10.1122/1.2890780

² Lin CC, Griffin PJ, Chao H, Hore MJA, Ohno K, Clarke N, et al. Grafted polymer chains suppress nanoparticle diffusion in athermal polymer melts. *J Chem Phys.* 2017;146(20):203332. doi: 10.1063/1.4982216

³ Kalathi JT, Yamamoto U, Schweizer KS, Grest GS, Kumar SK. Nanoparticle Diffusion in Polymer Nanocomposites. *Phys Rev Lett.* 2014;112(10):108301. doi: 10.1103/PhysRevLett.112.108301

⁴ Asakura S, Oosawa F. Interaction between particles suspended in solutions of macromolecules. *J Polym Sci.* 1958;33(126):183-192. doi: 10.1002/pol.1958.1203312618

⁵ Hooper JB, Schweizer KS. Contact Aggregation, Bridging, and Steric Stabilization in Dense Polymer-Particle Mixtures. *Macromolecules.* 2005;38(21):8858-8869. doi: 10.1021/ma051318k

⁶ Hall LM, Jayaraman A, Schweizer KS. Molecular theories of polymer nanocomposites. *Curr Opin Solid State Mater Sci.* 2010;14(2):38-48. doi: 10.1016/j.cossms.2009.08.004

⁷ Zhou Y, Schweizer KS. PRISM Theory of Local Structure and Phase Behavior of Dense Polymer Nanocomposites: Improved Closure Approximation and Comparison with Simulation. *Macromolecules.* 2020;53(22):9962-9972. doi: 10.1021/acs.macromol.0c02077

⁸ Tang TY, Arya G. Anisotropic Three-Particle Interactions between Spherical Polymer-Grafted Nanoparticles in a Polymer Matrix. *Macromolecules.* 2017;50(3):1167-1183. doi: 10.1021/acs.macromol.6b01936